Current-induced spin polarization at metallic surfaces from first principles

Andrea Droghetti[1,*] and Ilya V. Tokatly[2,3,4,5]

[1]*School of Physics and CRANN, Trinity College, The University of Dublin, Dublin 2, Ireland*

[2]*Nano-Bio Spectroscopy Group and European Theoretical Spectroscopy Facility (ETSF), Departamento de Polímeros y Materiales Avanzados: Física, Química y Tecnología, Universidad del País Vasco (UPV/EHU), Avenida Tolosa 72, 20018 San Sebastián, Spain*

[3]*IKERBASQUE, Basque Foundation for Science, 48009 Bilbao, Spain*

[4]*Donostia International Physics Center (DIPC), 20018 Donostia–San Sebastián, Spain*

[5]*Department of Physics and Engineering, ITMO University, Saint Petersburg, Russia*

(Received 8 March 2023; revised 16 May 2023; accepted 19 May 2023; published 30 May 2023)

We present the results of first-principles calculations based on density functional theory estimating the magnitude of the current-induced spin polarization (CISP) at the surfaces of the 5*d* transition metals with fcc and bcc crystal structures. We predict that the largest surface CISP occurs for W and Ta, whereas CISP is considerably weaker for Pt and Au surfaces. We then discuss how CISP emerges over a length scale equal to a few atomic layers as opposed to the spin accumulation characteristic of the spin Hall effect, which is related to the materials' spin diffusion length. Finally, using our estimates for the CISP magnitude, we suggest that the spin density appearing near W surfaces in experiments is mostly due to CISP, whereas that at Pt surfaces stems from the Hall effect.

DOI: 10.1103/PhysRevB.107.174433

I. INTRODUCTION

Spin-charge conversion phenomena [1,2] mediated by spin-orbit coupling (SOC) have opened promising new pathways to control and detect electrons' spins for next-generation spintronic devices. Prominent examples of such conversion phenomena are current-induced spin polarization (CISP) [3] and its Onsager reciprocal effect. The conduction electrons of some nonmagnetic materials become spin polarized in the presence of a flowing dc charge current, and, in turn, a charge current is generated as a response to a nonequilibrium spin polarization.

CISP was predicted more than four decades ago [4] and first observed in tellurium [5]. Later, the phenomenon was investigated in a two-dimensional (2D) electron gas [6–9] and detected optically in semiconducting heterostructures [10–15]. CISP in these 2D systems is called the Rashba-Edelstein effect or, equivalently, the inverse spin-galvanic effect. Recently, CISP has also been reported in the semimetallic $TaSi_2$ (Ref. [16]), while the possibility of modulating the effect through electrostatic gating has been demonstrated in Te nanowires [17]. Yet, to date, CISP has mostly been studied in 4*d* and 5*d* transition metal films, where a homogeneous spin polarization emerges at surfaces and interfaces [18]. When one of these 4*d* or 5*d* films is in proximity to a ferromagnet, the interfacial CISP can exert a torque on the ferromagnet's magnetization [19–21]. This type of spin-orbit torque [22] was predicted in early model calculations by Manchon and Zhang [23] and has extensively been studied as a means to write information in magnetoresistive random access memories (RAMs) [24]. Along with CISP, its reciprocal effect, often called the spin-galvanic effect, has also been demonstrated and extensively studied in many materials. The experiments initially considered semiconductor quantum wells [25–27], while, more recently, the focus has shifted towards metallic interfaces [28–33], metal-insulator interfaces [34,35], topological insulators [36], van der Waals heterostructures [37], and the 2D electron gas forming at oxide interfaces [38–40].

In spite of the large number of studies dedicated to CISP, reliable estimates of its magnitude in materials remain scarce. In device experiments, the spin polarization is not directly measurable, and it is extrapolated from electrical signals via complex analyses and fits to effective models [41–43]. As such, the conclusions are often controversial [44]. The problem becomes even more significant in the case of 4*d* and 5*d* transition metals and their heterostructures with ferromagnetic layers. In these systems, surface and interfacial CISP is often accompanied by the spin Hall effect (SHE) [45,46]. Although the SHE is a bulk phenomenon, it manifests itself at surfaces as a spin accumulation, which adds up to the CISP. In practice, separating the CISP from the spin accumulation due to the SHE is a challenging and debated problem [47–50]. Recently, attempts to directly measure the magnitude of CISP at metal surfaces were made in spin-polarized positron beam experiments [18,51], but the reported values appear surprisingly large.

Given the outstanding difficulties in extracting the CISP magnitude from experiments, first-principles calculations could potentially be very helpful to get benchmark results, as shown in some previous works for bulk Te, $TaSi_2$ (Ref. [52]), and the (111) surface of gold [53]. Furthermore, CISP in bulk materials was recently analyzed in Ref. [54], screening all

*andrea.droghetti@tcd.ie

 ©2023 American Physical Society

the nonmagnetic crystallographic space groups. However, to our knowledge, there have been no calculations for the most common materials used in experiments, namely, Pt and W, or, in fact, for any other transition metal (besides Au), where CISP takes place at surfaces. The purpose of this paper is then to close this knowledge gap.

We use first-principles calculations based on density functional theory (DFT) to quantitatively estimate the magnitude of CISP at the surfaces of the most investigated $5d$ transition metals. We obtain the charge current and the corresponding spatial-dependent spin density in thick slabs by populating the electronic bands as implied by the relaxation time approximation for electron transport. Our results indicate that the largest CISP occurs for W surfaces, and, furthermore, they provide some insight into how CISP can be distinguished from the SHE. Specifically, we show that the two phenomena lead to a nonequilibrium spin density extending over different length scales, and we point out for what materials CISP might be more significant than the SHE.

The paper is organized as follows. We start in Sec. II by reviewing the basic CISP phenomenology. We then provide the details of our DFT calculations in Sec. III, and we analyze the results in Sec. IV. Finally, we compare CISP and the SHE in Sec. V, before summarizing the main conclusion of our study in Sec. VI.

II. CISP: QUALITATIVE DESCRIPTION

CISP is described by the equation [3]

$$S^a = \gamma_b^a j_b, \quad a, b = x, y, z, \tag{1}$$

which linearly couples the nonequilibrium spin density $\mathbf{S} = (S^x, S^y, S^z)$ to the charge current density $\mathbf{j} = (j_x, j_y, j_z)$ (note that we here employ Einstein's convention of repeated indices). The coefficients γ_b^a, which effectively describe the CISP magnitude, are material specific. Nonetheless, we note that the emergence of CISP in a system is completely determined by symmetry. From a mathematical point of view, $\mathbf{j}$ and $\mathbf{S}$ are a polar and an axial vector, respectively. Thus γ_b^a is a component of a second-rank pseudotensor $\boldsymbol{\gamma}$. Nonzero second-rank pseudotensors are allowed by symmetry only in systems whose structure is characterized by a gyrotropic point symmetry group [3]. In other words, this means that CISP can be present only in gyrotropic media, first studied for their natural optical activity [55]. Gyrotropic point groups are listed, for example, in Ref. [56]. They form a subset of noncentrosymmetric groups; that is, not all noncentrosymmetric groups are gyrotropic. Thus breaking inversion symmetry in a system is not enough to observe CISP, and the symmetry requirements are more stringent. The materials where CISP can be observed either are chiral, are polar, have the $\mathbb{S}_4$ point group, or have the $\mathbb{D}_{2d}$ point group. A high-throughput analysis of CISP in bulk materials was recently carried out by Tenzin *et al.* [54], screening all the nonmagnetic crystallographic space groups.

Transition metals have nongyrotropic crystal structures. Hence CISP is absent as a bulk effect. However, CISP emerges at surfaces and interfaces which are locally gyrotropic. Equation (1) can still be assumed valid with $\mathbf{S}$ being the surface spin density (i.e., the spin density integrated over the coordinate perpendicular to the surface) and $\mathbf{j}$ being the bulk current density [53]. In the literature, the effect has often been associated with surface bands with spin textures in momentum space and modeled in terms of the 2D Rashba-Edelstein effect [28]. Such a description may, however, not be complete. For instance, in Au(111) films, the Shockley surface states show a large Rashba spin splitting [57], but their contribution to the total surface spin density is found to be minor [53]. The largest contribution originates from the continuum of bulk states scattering off the surface [53,58]. The effect is very reminiscent of the Friedel oscillations of the charge density. For a semi-infinite jellium model, taken to be representative of metals, the induced spin density is confined at the surface over a distance of the order of k_F^{-1}, where k_F is the Fermi wave vector (of the order of a few angstroms), and rapidly decays inside the bulk. For real thin films, accurate predictions of CISP at surfaces are only possible by means of detailed microscopic calculations, which take into account the effect of the atomic SOC on both bulk and surface electronic states. This is done in the following sections.

III. COMPUTATIONAL DETAILS

The DFT calculations are performed by means of a development version of the SIESTA code [59]. We use the local spin density approximation (LSDA) for the exchange-correlation density functional [60,61]. The SOC is included by means of the on-site approximation of Ref. [62], which we have generally found accurate even for materials with complex spin textures (e.g., Ref. [63]). We treat core electrons with norm-conserving Troullier-Martins pseudopotentials [64,65]. The valence states are expanded through a numerical atomic orbital basis set including multiple-ζ and polarization functions. The cutoff radii of the basis orbitals for Ta, W, and Pt are obtained from Ref. [66]. The cutoff radii of the basis orbitals of Ir and Pt are the same. For all systems, the pseudopotentials and basis sets have been validated to closely reproduce the band structures calculated with the QUANTUM ESPRESSO plane-wave code [67].

We consider the stable crystal structures and the experimental lattice vectors for all materials. In order to describe thin films, we carry out the calculations for slabs with an in-plane unit cell and whose thicknesses vary between 24 and 46 layers depending on the system. Assuming the relaxation time approximation [53], the current is introduced by populating with electrons the Kohn-Sham electronic bands of energy $E_{n,\mathbf{k}}$ and momentum $\hbar\mathbf{k}$ according to a displaced Fermi distribution $f(E_{n,\mathbf{k}} - \mathbf{v}_d\mathbf{k}) = [e^{-\beta(E_{n,\mathbf{k}} - E_F - \hbar\mathbf{v}_d\mathbf{k})} + 1]^{-1}$, where $\mathbf{v}_d$ is the electron drift velocity. The charge current is then evaluated through the "bond currents" method as explained in Refs. [68,69]. In our calculations, the drift velocity is taken as an input parameter, which is varied to obtain any desired output charge current density. A drift velocity of 1 m/s gives a current density of the order of 10^6 A/cm^2. We accurately verified that the output current density depends linearly on the input drift velocity in the calculations. We employ 101×101 $\mathbf{k}$ points in the two-dimensional surface Brillouin zone. SIESTA returns the spin density $\mathbf{s}(x, y, z)$ on a real-space grid. Here we use a very dense grid, specified via a mesh cutoff equal to 1000 Ry, for accurately resolving the spin density oscillations. For

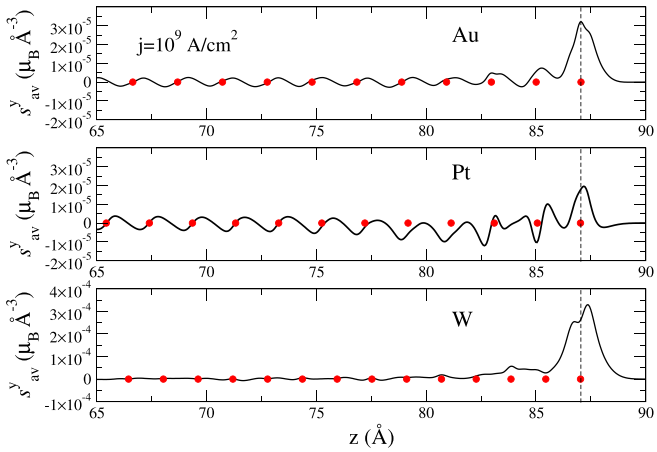

FIG. 1. Spin-y density $s^y_{\rm av}(z)$ of Au(001), Pt(001), and W(001) calculated for an applied current density $j_x = 10^9$ A/cm^2 along the x direction parallel to the surface. The atom positions along z are indicated by the red circles. The dashed line marks the position of the surface. Note the different scales used along the vertical axis in the three panels.

all materials we check that the obtained surface spin density is converged with respect to the slab thickness.

IV. DFT RESULTS

We investigate the $5d$ transition metals with room temperature equilibrium crystal structures which are either fcc (Au, Pt, Ir) or bcc (Ta, W). The calculations are performed for ideal slabs with a vacuum outside. Unless stated otherwise, we consider the (001) surfaces, which are described by the gyrotropic point group $\mathbb{C}_{4v}$. We assume a Cartesian frame of reference such that the x and y axes coincide with the (110) and (1$\bar{1}$0) crystal directions. The surface normal lies along the z axis, and we indicate the normal unit vector as $\mathbf{z}$. The only nonzero components of the pseudotensor $\boldsymbol{\gamma}$ allowed by symmetry in Eq. (1) are γ^x_y and γ^y_x, and additionally, $\gamma^x_y = \gamma^y_x \equiv \gamma$. Thus Eq. (1) can be rewritten as $\mathbf{S} = \gamma \mathbf{z} \times \mathbf{j}$ (Ref. [53]), where $\mathbf{S}$ is the surface spin density. The calculations are carried out in such a way that the charge current is along the x (y) direction. We then obtain the in-plane average spin-y (spin-x) density, also called "spin density profile," $s^{y(x)}_{\rm av}(z) = \int dxdy\, s^{y(x)}(x, y, z)/\mathcal{A}$, where $\mathcal{A}$ is the unit cell area in the xy plane. Finally, the surface spin density $S^{y(x)}$ is obtained by integrating $s^{y(x)}_{\rm av}(z)$ from the center of the slab to the vacuum region outside one of the slab's surfaces. We verified that the numerical calculations give $s^y_{\rm av}(z) = s^x_{\rm av}(z) \equiv s_{\rm av}(z)$ for $j_x = j_y$ as expected because of the systems' symmetry.

The calculated spin density profile for a current density equal to 10^9 A/cm^2 is plotted in Fig. 1 for three representative systems, namely, Au(001), Pt(001), and W(001). Such large current density is merely chosen for display reasons so that no numerical noise is visible in the curves. Nonetheless, since the surface spin density depends linearly on the current density according to Eq. (1), the density profiles corresponding to any other current density value can be readily obtained just by rescaling the plots accordingly. The red circles mark the position of the atoms along the z direction. The surface is located at $z = z_S \sim 87$ Å (dashed vertical line), and the vacuum extends from there towards $z = +\infty$. At the qualitative level, $s^y_{\rm av}(z)$ looks quite similar in the three materials. It presents a peak at the surface atomic layer (located at $z_S \sim 87$ Å) accompanied by an identical and opposite peak at the other slab surface (not shown). It then decays from the surface to the interior of the slab within about four atomic layers. Inside the slab, it assumes a periodic (almost sinusoidal) behavior with the period equal to the lattice spacing. In other words, we see the formation of a spin dipole with the positive and negative polarities centered between the atoms and integrating to zero over the bulk unit cell. CISP is therefore absent as a bulk unit cell property. It instead emerges at the surface layers because of the microscopic local gyrotropy. This behavior is the same as that found for another SOC-driven effect associated with gyrotropy, namely, non-Abelian diamagnetism [68,70]. In that case, one can calculate the effect's characteristic quantity, which is the equilibrium spin current [71], and show that it is finite at surfaces but it vanishes when integrated over the bulk unit cell [68] in the very same way as the spin density in CISP does.

The quantitative comparison of the results in Fig. 1 shows that the surface layer's spin density of the W slab is $s_{\rm av}(z_S) \sim 10^{-4}\ \mu_B/$Å^3, which is an order of magnitude larger than that of the Au and Pt slabs, $s_{\rm av}(z_S) \sim 10^{-5}\ \mu_B/$Å^3 (note the different scales used in the three panels of Fig. 1). These values can be compared with the results reported in Ref. [52] for Te. For the same current density considered here, the spin density in Te is extrapolated to be approximately $10^{-1}\ \mu_B/$Å^3, i.e., several orders of magnitude larger than in our $5d$ metal surfaces. The surface CISP due to local gyrotropy in an otherwise centrosymmetric system is generally a much weaker effect than CISP in materials with bulk gyrotropic symmetry.

To see whether our estimates may depend on the surface cut, we performed additional calculations for (111) slabs. Overall, for all three materials, we find that the surface layer's spin density and the integrated surface spin density have values similar to those for the (001) case, although the spin density profile may be locally different. Once the spin density profiles are integrated, we obtain that the total spin density $S^{y(x)}$ is about $10^4\ \mu_B/$cm^2 for W, while it is $S^{y(x)} \approx 10^3\ \mu_B/$cm^2 for Au and Pt. These are small values, but, as stated in Ref. [53], they could in principle be measured in optical experiments with the current resolution.

A systematic comparison of the surface CISPs across the various considered $5d$ materials is done by plotting in Fig. 2 the parameter $\gamma \equiv \gamma^x_y = \gamma^y_x$ of Eq. (1) (see the black circles). In the case of Ta, we also consider the so-called β phase, which is commonly regarded as a high-performing material for spin-charge conversion [72,73]. The most striking conclusion that can be drawn based on the results is that the surface CISP in Ta and W is about an order of magnitude larger than in the late $5d$ materials. Specifically, we get that γ is about $10^3\ \mu_B/$A for Ta and W, while it is $10^2\ \mu_B/$A for Pt and Au. This might indicate that there could be a correlation between CISP and the Hund's coupling, although we must stress that CISP depends on the fine details of the slabs' intricate band structure, which is populated according to the out-of-

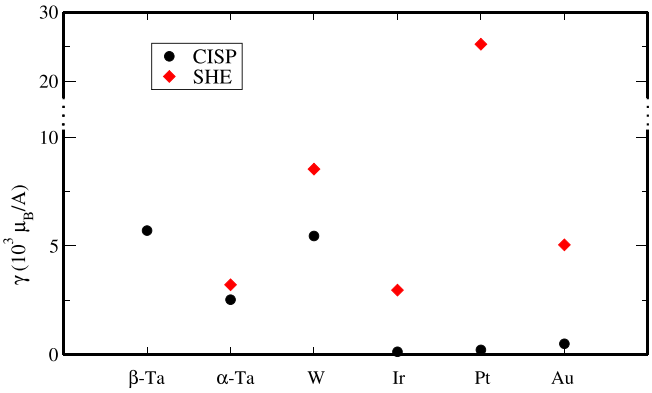

FIG. 2. Surface CISP (SHE) factor γ ($\gamma_{\rm SHE}$) for the various investigated 5d metals.

equilibrium electron distribution. A simple interpretation of the results based on a single atomic property is therefore not possible. Yet, looking at our calculations, we can suggest that spintronic devices aiming at exploiting surface CISP should be made of either Ta or W films to achieve the best possible performance.

Although our results are obtained for ideal surfaces with a vacuum, we think that they will remain valid also for systems with rough surfaces or in contact with layers of other materials, as found in experiments. Disorder at the surface layer will decrease the in-plane symmetry, but any heterointerface is intrinsically a polar system (it allows for a polar vector, normal to the surface) and, as such, is always gyrotropic. In the limit of full disorder, a surface layer will become, on average, isotropic. This formally corresponds to the $\mathbb{C}_{\infty v}$ point group, which has the same symmetry as the Rashba model, and therefore it allows for CISP with the same directional character as found for our ideal systems. In the case of a surface in contact with another material, the band structure of the surface layer would be strongly modified by the bonding with the adjacent layer. However, based on the results of Ref. [53] for Au, we believe that surface CISP in 5d metals is due mostly to bulk states scattering off the surface, while surface or interface states play a less important role. As such, the magnitude of the spin density profile would not drastically change in multilayer samples compared with our ideal systems.

Recently, spin-polarized positron beam experiments were performed to directly probe CISP at some 5d metal surfaces [18]. To compare our calculations with these experimental results, we define the spin polarization (SP) as the spin density divided by the charge density in proximity to the surface layer. The largest calculated SP is obtained for W and is equal to about 10^{-5} for a charge current density as large as in experiments (10^5 A/cm^2). This SP is several orders of magnitude smaller than the experimentally reported one, which is about 0.1. Overall, all experimental values appear surprisingly large, and even much larger than the results in Refs. [17,52] for bulk Te, which, as mentioned above, is a "strong" gyrotropic material and is expected to show enhanced CISP compared with any metallic surfaces. Resolving such disagreements between the calculated and measured SP will represent an important issue for potential future studies.

V. CISP VERSUS THE SPIN HALL EFFECT

We now turn to the question of the importance of CISP with respect to the SHE in 5d metallic films. To determine the relative magnitude of the two phenomena, we just need to quantify the spin accumulation induced by the SHE and compare it with the calculated spin density due to CISP.

We consider a semi-infinite system along the z direction, with the surface located at a position $z = z_S$, and a vacuum extending from z_S towards $z = +\infty$. The charge current j_x flows along the x direction as in the CISP calculations above. Assuming diffusive spin dynamics, the SHE induces a z-dependent spin current and a spin density that are given by the equations [74,75]

$$j_z^y(z) = \left[\theta_{\rm SHE} j_x - D\partial_z s^y_{\rm SHE}(z)\right], \tag{2}$$

$$\partial_z^2 s^y_{\rm SHE}(z) - \frac{1}{l_{\rm SD}^2} s^y_{\rm SHE}(z) = 0, \tag{3}$$

where $\theta_{\rm SHE}$ is the bulk spin Hall angle, $l_{\rm SD}$ is the bulk spin diffusion length, and D is the bulk diffusion constant. These equations are decoupled from Eq. (1) because the interface CISP enters the drift-diffusion theory as an effective boundary condition [75]. Internal consistency requires that it modifies only the computation of the surface spin but does not change the calculation of the bulk "diffusive spin." Hence, in the limits of validity of the drift-diffusion theory, the bulk spin accumulation due to SHE can be calculated independently of the surface CISP. In simple words, in the experimentally relevant linear regime, the SHE and the surface CISP are two physically distinct mechanisms for the generation of the integrated surface spin density; their response coefficients can be obtained separately, and add up.

Equation (3) implies that the spin density stemming from the SHE vanishes exponentially from the surface towards the bulk of the system, and the solution reads

$$s^y_{\rm SHE}(z) = s e^{-(z_S - z)/l_{\rm SD}}, \quad z \leqslant z_S, \tag{4}$$

where s is the spin density at the surface, i.e., at $z = z_S$. Equation (2) must be accompanied by the boundary condition $j_z^y|_{z=z_S} = 0$, which enforces that the spin current vanishes at the surface as it cannot flow into the vacuum region. Thus the integrated spin density is

$$S^y_{\rm SHE} = \gamma_{\rm SHE} j_x \tag{5}$$

and defines the spin accumulation due to the SHE. The parameter $\gamma_{\rm SHE} = \theta_{\rm SHE} l_{\rm SD}^2/D$ expresses the magnitude of the spin density induced only by the SHE as opposed to γ in Eq. (1) that uniquely characterizes CISP. $\gamma_{\rm SHE}$ can be directly computed provided that $\theta_{\rm SHE}$, $l_{\rm SD}$, and D are known to a reasonable accuracy. Unfortunately, however, the reported values for these quantities vary widely from experiment to experiment [45,46] likely because of the different crystalline quality of the measured samples and unavoidable extrinsic contributions from disorder or impurities [76]. We therefore employ here the theoretical estimates provided by Nair *et al.* in Ref. [77], which are based on scattering theory combined with DFT. The calculated values of $\gamma_{\rm SHE}$ are presented in Fig. 2 as red diamonds. No data are available for β-Ta.

In Ta and W, γ_{SHE} is almost as large as the CISP factor γ. This means that the integrated spin density induced by the SHE and CISP are comparable in these materials. However, it is important to point out the different length scales over which the spin density is localized. In CISP, the spin density is mostly confined within a few atomic layers around the surface (see Fig. 1), i.e., over a length $l_{CISP} \approx 1$ nm. In contrast, in the SHE the spin density is accumulated over a characteristic length dictated by the spin diffusion length. In the case of W, l_{SD} is 29.6 nm (about 140 atomic layers). This means that at the surface layer, $s_{SHE}/s_{CISP} \approx l_{CISP}/l_{SD} \approx 3 \times 10^{-2}$. The spin density originating from CISP is two orders of magnitude larger than that due to the SHE, or in other words, the contribution of the SHE in W is negligible compared with that of CISP. Similar considerations also apply to Ta, although we obtain $s_{SHE}/s_{CISP} \approx 10^{-1}$ since l_{SD} is much smaller (6.16 nm) than in W. Nonetheless, we must point out that the spin Hall angles of W and Ta taken from Ref. [77] are very small, i.e., $\theta_{SHE} \approx 0.4$ and 0.5. While the value for Ta appears to be in fair agreement with the experimental results [73], in the case of W, the experimental estimates for θ_{SHE} span from 0 to 5% (Refs. [78,79]). A theoretical evaluation of the intrinsic contribution based on the Berry curvature of the band structure gave 2% (Ref. [80]). Using this value, we would obtain a slight increase in the relevance of the SHE.

In the case of Au, γ_{SHE} is not vanishing in spite of the negligible spin Hall angle ($\theta_{SHE} = 0.25\%$). This is because of the huge spin diffusion length, $l_{SD} = 50.9$ nm. As a result, we find that $s_{SHE}/s_{CISP} \approx 0.5$. Thus, in Au, the SHE and CISP contributions to the surface spin density are somewhat comparable. Finally, in Pt, we find that $\gamma_{SHE} \approx 2.5 \times 10^4$ is much larger than in any other material because of the short spin diffusion length $l_{SD} = 5.21$ nm and of the large spin Hall angle ($\theta = 4.02\%$). Consequently, at the surface layer we obtain $s_{SHE}/s_{CISP} \approx 25$. This means that the surface spin density is mostly induced by the SHE rather than by CISP. Pt represents the opposite case of W. Some important experiments with Pt, where CISP due to the surface states was considered as the dominant contribution to the surface spin density [19], might need to be revisited in terms of the SHE.

VI. CONCLUSION

In conclusion, we provided an estimate of the CISP magnitude for several 5*d* metallic surfaces. The W surface shows the largest effect, while CISP is an order of magnitude smaller at the Pt and Au surfaces. We also showed that the spin density due to CISP may often be comparable to the spin accumulation induced by the SHE. However, the two effects appear at different length scales. In the case of W, the spin density at a film's surface layer is mostly due to CISP. In contrast, in the case of Pt, the surface spin density is caused mostly by the SHE. These observations may be valuable for the interpretation of experiments.

ACKNOWLEDGMENTS

A.D. was supported by Science Foundation Ireland and the Royal Society through University Research Fellowship No. URF-R1-191769 and by the European Commission through the H2020-EU.1.2.1 FET-Open project INTERFAST (Project No. 965046). I.V.T. acknowledges support from Grupos Consolidados UPV/EHU del Gobierno Vasco (Grant No. IT1453-22) and from Grant No. PID2020-112811GB-I00 funded by MCIN/AEI/10.13039/501100011033. The computational resources were provided by Trinity College Dublin Research IT.

[1] Y. Otani, M. Shiraishi, A. Oiwa, E. Saitoh, and S. Murakami, Nat. Phys. **13**, 829 (2017).
[2] W. Han, Y. Otani, and S. Maekawa, npj Quantum Mater. **3**, 27 (2018).
[3] S. D. Ganichev, M. Trushin, and J. Schliemann, in *Semiconductor Spintronics*, 2nd ed., edited by E. Y. Tsymbal and I. Žutić, Spintronics Handbook: Spin Transport and Magnetism Vol. 2 (CRC, Boca Raton, FL, 2019), pp. 317–338; arXiv:1606.02043.
[4] E. L. Ivchenko and G. E. Pikus, Pis'ma Zh. Eksp. Teor. Fiz. **27**, 640 (1978) [JETP Lett. **27**, 604 (1978)].
[5] L. Vorob'ev, E. Ivchenko, G. Pikus, I. I. Farbshtein, V. Shalygin, and A. Shturbin, Pis'ma Zh. Eksp. Teor. Fiz. **29**, 485 (1979) [JETP Lett. **29**, 441 (1979)].
[6] E. Ivchenko, Y. Lyanda-Geller, and Pikus, Pis'ma Zh. Eksp. Teor. Fiz. **50**, 156 (1989) [JETP Lett. **50**, 175 (1989)].
[7] A. Aronov and Y. Lyanda-Geller, Pis'ma Zh. Eksp. Teor. Fiz. **50**, 398 (1989) [JETP Lett. **50**, 431 (1989)].
[8] V. Edelstein, Solid State Commun. **73**, 233 (1990).
[9] L. Levitov, Y. Nazarov, and G. Eliashberg, Pis'ma Zh. Eksp. Teor. Fiz. **88**, 229 (1985) [Sov. Phys. JETP **61**, 133 (1985)].
[10] Y. K. Kato, R. C. Myers, A. C. Gossard, and D. D. Awschalom, Phys. Rev. Lett. **93**, 176601 (2004).
[11] Y. K. Kato, R. C. Myers, A. C. Gossard, and D. D. Awschalom, Science **306**, 1910 (2004).
[12] V. Sih, R. C. Myers, Y. K. Kato, W. H. Lau, A. C. Gossard, and D. D. Awschalom, Nat. Phys. **1**, 31 (2005).
[13] C. L. Yang, H. T. He, L. Ding, L. J. Cui, Y. P. Zeng, J. N. Wang, and W. K. Ge, Phys. Rev. Lett. **96**, 186605 (2006).
[14] H. J. Chang, T. W. Chen, J. W. Chen, W. C. Hong, W. C. Tsai, Y. F. Chen, and G. Y. Guo, Phys. Rev. Lett. **98**, 136403 (2007).
[15] B. M. Norman, C. J. Trowbridge, D. D. Awschalom, and V. Sih, Phys. Rev. Lett. **112**, 056601 (2014).
[16] K. Shiota, A. Inui, Y. Hosaka, R. Amano, Y. Ōnuki, M. Hedo, T. Nakama, D. Hirobe, J.-i. Ohe, J.-i. Kishine, H. M. Yamamoto, H. Shishido, and Y. Togawa, Phys. Rev. Lett. **127**, 126602 (2021).
[17] F. Calavalle, M. Suárez-Rodríguez, B. Martín-García, A. Johansson, D. C. Vaz, H. Yang, I. V. Maznichenko, S. Ostanin, A. Mateo-Alonso, A. Chuvilin, I. Mertig, M. Gobbi, F. Casanova, and L. E. Hueso, Nat. Mater. **21**, 526 (2022).
[18] H. J. Zhang, S. Yamamoto, Y. Fukaya, M. Maekawa, H. Li, A. Kawasuso, T. Seki, E. Saitoh, and K. Takanashi, Sci. Rep. **4**, 4844 (2014).

[19] I. M. Miron, T. Moore, H. Szambolics, L. D. Buda-Prejbeanu, S. Auffret, B. Rodmacq, S. Pizzini, J. Vogel, M. Bonfim, A. Schuhl, and G. Gaudin, Nat. Mater. **10**, 419 (2011).
[20] A. Ghosh, K. Garello, C. O. Avci, M. Gabureac, and P. Gambardella, Phys. Rev. Appl. **7**, 014004 (2017).
[21] X. Chen, Y. Liu, G. Yang, H. Shi, C. Hu, M. Li, and H. Zeng, Nat. Commun. **9**, 2569 (2018).
[22] A. Manchon, J. Železný, I. M. Miron, T. Jungwirth, J. Sinova, A. Thiaville, K. Garello, and P. Gambardella, Rev. Mod. Phys. **91**, 035004 (2019).
[23] A. Manchon and S. Zhang, Phys. Rev. B **78**, 212405 (2008).
[24] Q. Shao, P. Li, L. Liu, H. Yang, S. Fukami, A. Razavi, H. Wu, K. Wang, F. Freimuth, Y. Mokrousov, M. D. Stiles, S. Emori, A. Hoffmann, J. Åkerman, K. Roy, J.-P. Wang, S.-H. Yang, K. Garello, and W. Zhang, IEEE Trans. Magn. **57**, 800439 (2021).
[25] S. D. Ganichev, E. L. Ivchenko, S. N. Danilov, J. Eroms, W. Wegscheider, D. Weiss, and W. Prettl, Phys. Rev. Lett. **86**, 4358 (2001).
[26] S. D. Ganichev, E. L. Ivchenko, V. V. Bel'kov, S. A. Tarasenko, M. Sollinger, D. Weiss, W. Wegscheider, and W. Prettl, Nature (London) **417**, 153 (2002).
[27] S. Ganichev, S. Danilov, P. Schneider, V. Bel'kov, L. Golub, W. Wegscheider, D. Weiss, and W. Prettl, J. Magn. Magn. Mater. **300**, 127 (2006).
[28] J. C. R. Sánchez, L. Vila, G. Desfonds, S. Gambarelli, J. P. Attané, J. M. De Teresa, C. Magén, and A. Fert, Nat. Commun. **4**, 2944 (2013).
[29] S. Sangiao, J. M. De Teresa, L. Morellon, I. Lucas, M. C. Martinez-Velarte, and M. Viret, Appl. Phys. Lett. **106**, 172403 (2015).
[30] M. Isasa, M. C. Martínez-Velarte, E. Villamor, C. Magén, L. Morellón, J. M. De Teresa, M. R. Ibarra, G. Vignale, E. V. Chulkov, E. E. Krasovskii, L. E. Hueso, and F. Casanova, Phys. Rev. B **93**, 014420 (2016).
[31] A. Nomura, T. Tashiro, H. Nakayama, and K. Ando, Appl. Phys. Lett. **106**, 212403 (2015).
[32] M. Matsushima, Y. Ando, S. Dushenko, R. Ohshima, R. Kumamoto, T. Shinjo, and M. Shiraishi, Appl. Phys. Lett. **110**, 072404 (2017).
[33] R. Yu, B. Miao, Q. Liu, K. He, W. Xue, L. Sun, M. Wu, Y. Wu, Z. Yuan, and H. Ding, Phys. Rev. B **102**, 144415 (2020).
[34] S. Karube, K. Kondou, and Y. Otani, Appl. Phys. Express **9**, 033001 (2016).
[35] H. Tsai, S. Karube, K. Kondou, N. Yamaguchi, F. Ishii, and Y. Otani, Sci. Rep. **8**, 5564 (2018).
[36] Y. Shiomi, K. Nomura, Y. Kajiwara, K. Eto, M. Novak, K. Segawa, Y. Ando, and E. Saitoh, Phys. Rev. Lett. **113**, 196601 (2014).
[37] T. S. Ghiasi, A. A. Kaverzin, P. J. Blah, and B. J. van Wees, Nano Lett. **19**, 5959 (2019).
[38] E. Lesne, Y. Fu, S. Oyarzun, J. C. Rojas-Sánchez, D. C. Vaz, H. Naganuma, G. Sicoli, J.-P. Attané, M. Jamet, E. Jacquet, J.-M. George, A. Barthélémy, H. Jaffrès, A. Fert, M. Bibes, and L. Vila, Nat. Mater. **15**, 1261 (2016).
[39] Q. Song, H. Zhang, T. Su, W. Yuan, Y. Chen, W. Xing, J. Shi, J. Sun, and W. Han, Sci. Adv. **3**, e1602312 (2017).
[40] D. C. Vaz, P. Noël, A. Johansson, B. Göbel, F. Y. Bruno, G. Singh, S. McKeown-Walker, F. Trier, L. M. Vicente-Arche, A. Sander, S. Valencia, P. Bruneel, M. Vivek, M. Gabay, N. Bergeal, F. Baumberger, H. Okuno, A. Barthélémy, A. Fert, L. Vila *et al.*, Nat. Mater. **18**, 1187 (2019).
[41] S. Hong, V. Diep, S. Datta, and Y. P. Chen, Phys. Rev. B **86**, 085131 (2012).
[42] C. H. Li, O. M. J. van 't Erve, J. T. Robinson, Y. Liu, L. Li, and B. T. Jonker, Nat. Nanotechnol. **9**, 218 (2014).
[43] C. Sanz-Fernández, V. T. Pham, E. Sagasta, L. E. Hueso, I. V. Tokatly, F. Casanova, and F. S. Bergeret, Appl. Phys. Lett. **117**, 142405 (2020).
[44] J. Tian, S. Hong, S. Sayed, J. S. Lee, S. Datta, N. Samarth, and Y. P. Chen, Nat. Commun. **10**, 1461 (2019).
[45] J. Sinova, S. O. Valenzuela, J. Wunderlich, C. H. Back, and T. Jungwirth, Rev. Mod. Phys. **87**, 1213 (2015).
[46] A. Hoffmann, IEEE Trans. Magn. **49**, 5172 (2013).
[47] G. Allen, S. Manipatruni, D. E. Nikonov, M. Doczy, and I. A. Young, Phys. Rev. B **91**, 144412 (2015).
[48] Y. Du, H. Gamou, S. Takahashi, S. Karube, M. Kohda, and J. Nitta, Phys. Rev. Appl. **13**, 054014 (2020).
[49] J. Shen, Z. Feng, P. Xu, D. Hou, Y. Gao, and X. Jin, Phys. Rev. Lett. **126**, 197201 (2021).
[50] D. Yue, W. Lin, J. Li, X. Jin, and C. L. Chien, Phys. Rev. Lett. **121**, 037201 (2018).
[51] H. J. Zhang, S. Yamamoto, B. Gu, H. Li, M. Maekawa, Y. Fukaya, and A. Kawasuso, Phys. Rev. Lett. **114**, 166602 (2015).
[52] A. Roy, F. T. Cerasoli, A. Jayaraj, K. Tenzin, M. B. Nardelli, and J. Sławińska, npj Comput. Mater. **8**, 243 (2022).
[53] I. V. Tokatly, E. E. Krasovskii, and G. Vignale, Phys. Rev. B **91**, 035403 (2015).
[54] K. Tenzin, A. Roy, H. Jafari, B. Banas, F. T. Cerasoli, M. Date, A. Jayaraj, M. Buongiorno Nardelli, and J. Sławińska, Phys. Rev. B **107**, 165140 (2023).
[55] L. Landau, L. Pitaevskii, and E. Lifshitz, *Electrodynamics of Continuous Media* (Elsevier, New York, 1984).
[56] W.-Y. He and K. T. Law, Phys. Rev. Res. **2**, 012073(R) (2020).
[57] S. LaShell, B. A. McDougall, and E. Jensen, Phys. Rev. Lett. **77**, 3419 (1996).
[58] P. Bokes and F. Horváth, Phys. Rev. B **81**, 125302 (2010).
[59] J. M. Soler, E. Artacho, J. D. Gale, A. García, J. Junquera, P. Ordejón, and D. Sánchez-Portal, J. Phys.: Condens. Matter **14**, 2745 (2002).
[60] U. von Barth and L. Hedin, J. Phys. C **5**, 1629 (1972).
[61] S. H. Vosko, L. Wilk, and M. Nusair, Can. J. Phys. **58**, 1200 (1980).
[62] L. Fernández-Seivane, M. A. Oliveira, S. Sanvito, and J. Ferrer, J. Phys.: Condens. Matter **18**, 7999 (2006).
[63] S. Jakobs, A. Narayan, B. Stadtmüller, A. Droghetti, I. Rungger, Y. S. Hor, S. Klyatskaya, D. Jungkenn, J. Stöckl, M. Laux, O. L. A. Monti, M. Aeschlimann, R. J. Cava, M. Ruben, S. Mathias, S. Sanvito, and M. Cinchetti, Nano Lett. **15**, 6022 (2015).
[64] N. Troullier and J. L. Martins, Phys. Rev. B **43**, 1993 (1991).
[65] N. Troullier and J. L. Martins, Phys. Rev. B **43**, 8861 (1991).
[66] P. Rivero, V. M. García-Suárez, D. Pereñiguez, K. Utt, Y. Yang, L. Bellaiche, K. Park, J. Ferrer, and S. Barraza-Lopez, Comput. Mater. Sci. **98**, 372 (2015).
[67] P. Giannozzi, S. Baroni, N. Bonini, M. Calandra, R. Car, C. Cavazzoni, D. Ceresoli, G. L. Chiarotti, M. Cococcioni, I. Dabo, A. Dal Corso, S. de Gironcoli, S. Fabris, G. Fratesi, R. Gebauer, U. Gerstmann, C. Gougoussis, A. Kokalj, M. Lazzeri,

L. Martin-Samos *et al.*, J. Phys.: Condens. Matter **21**, 395502 (2009).
[68] A. Droghetti, I. Rungger, A. Rubio, and I. V. Tokatly, Phys. Rev. B **105**, 024409 (2022).
[69] I. Rungger, A. Droghetti, and M. Stamenova, in *Methods: Theory and Modeling*, Handbook of Materials Modeling Vol. 1, edited by S. Yip and W. Andreoni (Springer, Cham, Switzerland, 2020), pp. 957–983.
[70] I. V. Tokatly, Phys. Rev. Lett. **101**, 106601 (2008).
[71] E. I. Rashba, Phys. Rev. B **68**, 241315(R) (2003).
[72] L. Liu, C.-F. Pai, Y. Li, H. W. Tseng, D. C. Ralph, and R. A. Buhrman, Science **336**, 555 (2012).
[73] E. Sagasta, Y. Omori, S. Vélez, R. Llopis, C. Tollan, A. Chuvilin, L. E. Hueso, M. Gradhand, Y. C. Otani, and F. Casanova, Phys. Rev. B **98**, 060410(R) (2018).
[74] M. I. Dyakonov and A. V. Khaetskii, in *Spin Physics in Semiconductors*, 2nd ed. (Springer, Berlin, 2017), Chap. 8, pp. 211–244.
[75] J. Borge and I. V. Tokatly, Phys. Rev. B **99**, 241401(R) (2019).
[76] E. Sagasta, Y. Omori, M. Isasa, M. Gradhand, L. E. Hueso, Y. Niimi, Y. Otani, and F. Casanova, Phys. Rev. B **94**, 060412(R) (2016).
[77] R. S. Nair, E. Barati, K. Gupta, Z. Yuan, and P. J. Kelly, Phys. Rev. Lett. **126**, 196601 (2021).
[78] D. Qu, S. Y. Huang, B. F. Miao, S. X. Huang, and C. L. Chien, Phys. Rev. B **89**, 140407(R) (2014).
[79] K. Fritz, S. Wimmer, H. Ebert, and M. Meinert, Phys. Rev. B **98**, 094433 (2018).
[80] X. Sui, C. Wang, J. Kim, J. Wang, S. H. Rhim, W. Duan, and N. Kioussis, Phys. Rev. B **96**, 241105(R) (2017).